Science Advances
AAAS

Supplementary Materials for

High-throughput and high-content bioassay enables tuning of polyester nanoparticles for cellular uptake, endosomal escape, and systemic in vivo delivery of mRNA

Yuan Rui, David R. Wilson, Stephany Y. Tzeng, Hannah M. Yamagata, Deepti Sudhakar, Marranne Conge, Cynthia A. Berlinicke, Donald J. Zack, Anthony Tuesca, Jordan J. Green*

*Corresponding author. Email: green@jhu.edu

Published 5 January 2022, *Sci. Adv.* **8**, eabk2855 (2022)
DOI: 10.1126/sciadv.abk2855

This PDF file includes:

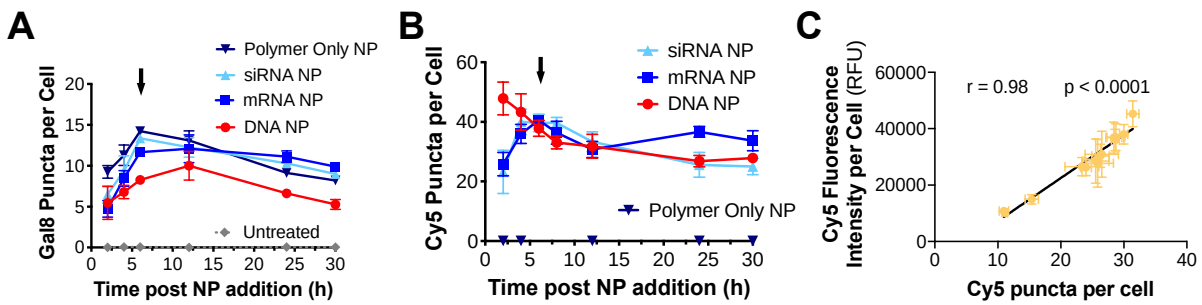

Figure S1. Optimization for dual NP uptake/Gal8 endosomal disruption assay. (A) Gal8 puncta count and **(B)** Cy5 puncta count for 7-90,c12-63, 50%-Sc12 NPs delivering various nucleic acid cargos to B16-F10 cells after different incubation times. Black arrow indicates the 6 h time point, which was chosen as the NP incubation time for this assay. **(C)** Overall intracellular Cy5 fluorescence as a function of Cy5 puncta count per cell for mRNA nanoparticles formulated with all PBAE polymers tested. Correlation significance was assessed using Spearman's method, and significant correlations were indicated with fitted lines. Data presented as mean ± SD, $n = 4$.

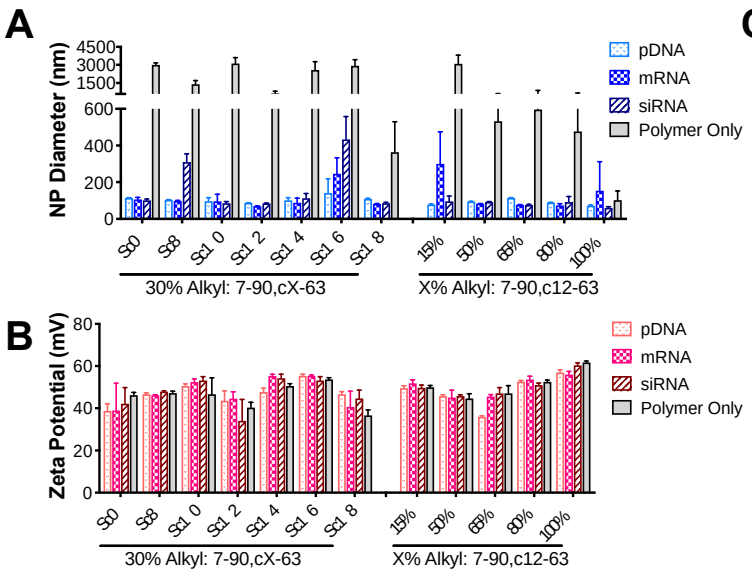

C

	Polymer ID	Alkyl Amine Content (mol %)	Number Average Molecular Weight (kD)	MW PDI
30% Alkyl: 7-90,cX-63	Sc0	None	7277	2.20
	Sc8	30% Sc8	4358	1.15
	Sc10	30% Sc10	9330	3.05
	Sc12	30% Sc12	4446	2.66
	Sc14	30% Sc14	7578	2.05
	Sc16	30% Sc16	8774	3.07
	Sc18	30% Sc18	8759	3.03
X% Alkyl: 7-90,c12-63	15%	15% Sc12	7473	1.62
	50%	50% Sc12	4464	2.66
	65%	65% Sc12	5820	2.50
	80%	80% Sc12	7217	2.38
	100%	100% Sc12	5083	1.80

Figure S2. Polymer and nanoparticle characteristics for the polymer backbone hydrophobicity variation series. (A) Z-average hydrodynamic diameter and **(B)** zeta potential for polymers encapsulating plasmid DNA, mRNA, siRNA, or polymer only nanoparticles (no nucleic acids). Data shown as mean ± SD, *n* = 3. **(C)** Polymer molecular weight as determined by GPC.

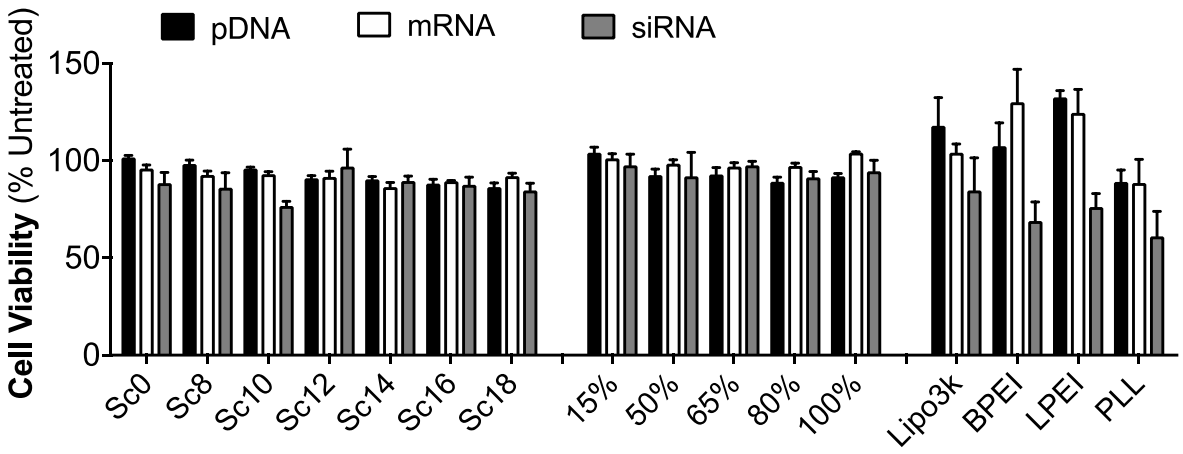

Figure S3. B16-F10 cell viability after treatment with nanoparticles encapsulating different nucleic acid cargos. Viability calculated by normalizing the cell count in treated wells to that of untreated wells. Data presented as mean ± SD, *N*=4.

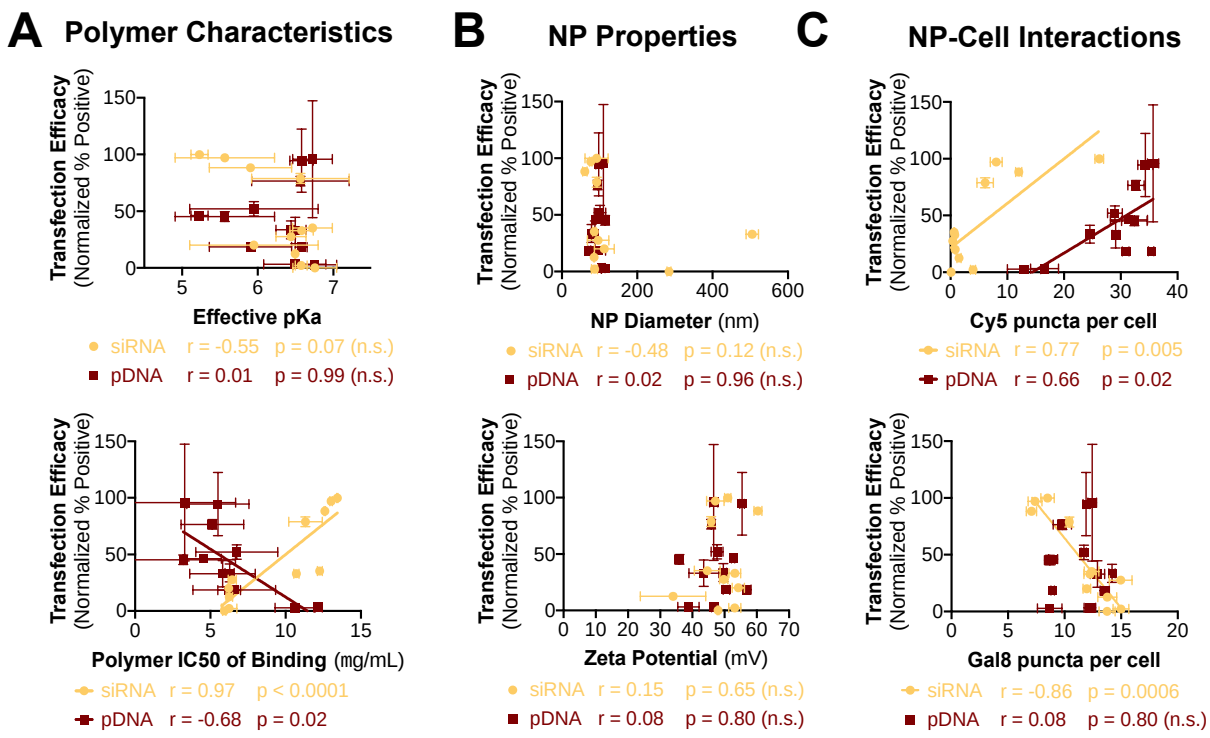

Figure S4. Correlations between transfection efficacy and polymer characteristics, nanoparticle properties, and nanoparticle-cell interactions. Transfection efficacy of nanoparticles formed with PBAE polymers encapsulating DNA or siRNA was plotted against common predictor readouts such as **(A)** various polymer characteristics, **(B)** nanoparticle properties, and **(C)** nanoparticle-cell interactions. Correlation significance was assessed using Spearman's method, and data sets with statistically significant correlations were indicated with fitted lines. Data presented as mean ± SD, *N*=4.

A

	Polymer ID	Effective pKa
30% Alkyl: 7-90,cX-63	Sc0	6.7 ± 0.1
	Sc8	6.6 ± 0.01
	Sc10	6.5 ± 0.01
	Sc12	6.5 ± 0.01
	Sc14	6.5 ± 0.1
	Sc16	6.7 ± 0.04
	Sc18	6.7 ± 0.2
X% Alkyl: 7-90,c12-63	15% Sc12	6.3 ± 0.1
	50% Sc12	6.2 ± 0.1
	65% Sc12	5.6 ± 0.7
	80% Sc12	5.0 ± 0.1
	100% Sc12	5.3 ± 0.6

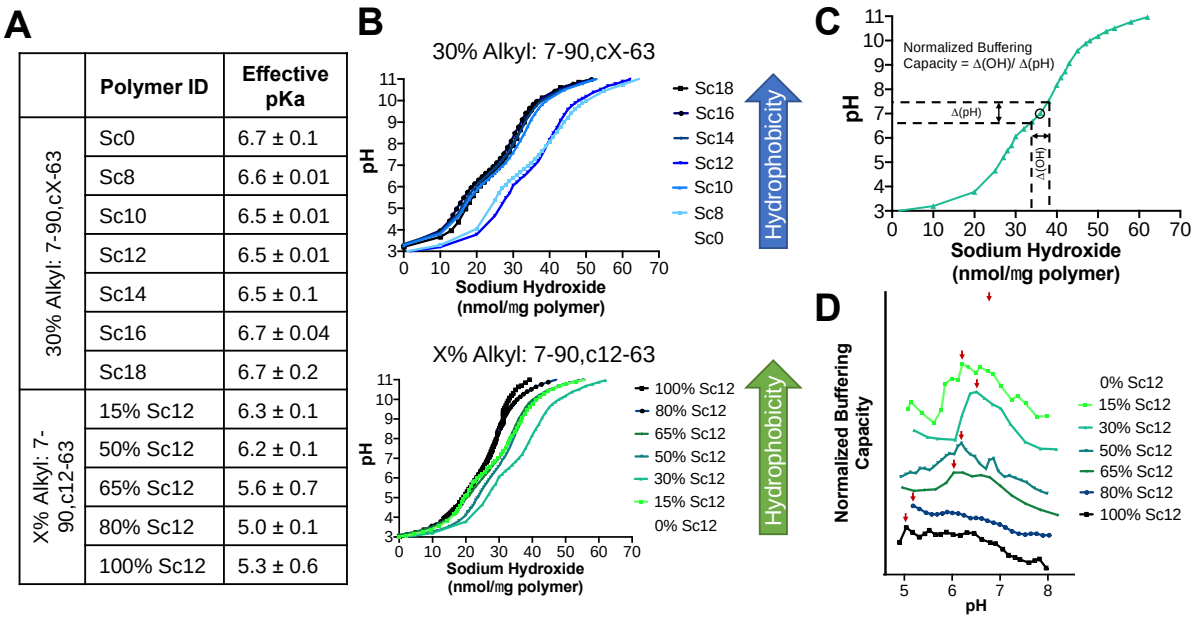

Figure S5. Polymer effective pKa and pH titration curves. (A) Effective pKa in the physiologically relevant pH range for polymers in the backbone variation series. **(B)** Representative pH titration curves. **(C)** Normalized buffering capacity was calculated from pH titration data as Δ(OH)/ Δ(pH) at each titration point (pH 5-8). **(D)** Effective pKa value of each polymer was determined as the pH point of the maximum normalized buffering capacity (indicated by red arrows in representative curves).

A

	Polymer ID	Polymer IC50 of Binding (μg/mL)		
		pDNA	mRNA	siRNA
30% Alkyl: 7-90,cX-63	Sc0	12.2 ± 0.2	4.0 ± 0.7	5.8 ± 0.1
	Sc8	10.6 ± 0.9	3.15 ± 0.04	5.9 ± 0.1
	Sc10	6.3 ± 0.5	4.3 ± 0.3	6.2 ± 0.4
	Sc12	6 ± 2	4.23 ± 0.03	6.3 ± 0.1
	Sc14	7 ± 2	4.03 ± 0.01	6.6 ± 0.4
	Sc16	6 ± 1	3.99 ± 0.06	10.8 ± 0.1
	Sc18	3 ± 2	3.6 ± 0.2	12.2 ± 0.1
X% Alkyl: 7-90,c12-63	15% Sc12	6.3 ± 0.2	3.0 ± 0.2	6.5 ± 0.2
	50% Sc12	5 ± 1	5.8 ± 0.7	11.4 ± 0.5
	65% Sc12	3 ± 2	7.1 ± 0.8	13.1 ± 0.1
	80% Sc12	4.5 ± 0.9	1.6 ± 0.4	13.1 ± 0.3
	100% Sc12	7± 2	1.1 ± 0.5	12.7 ± 0.1

B

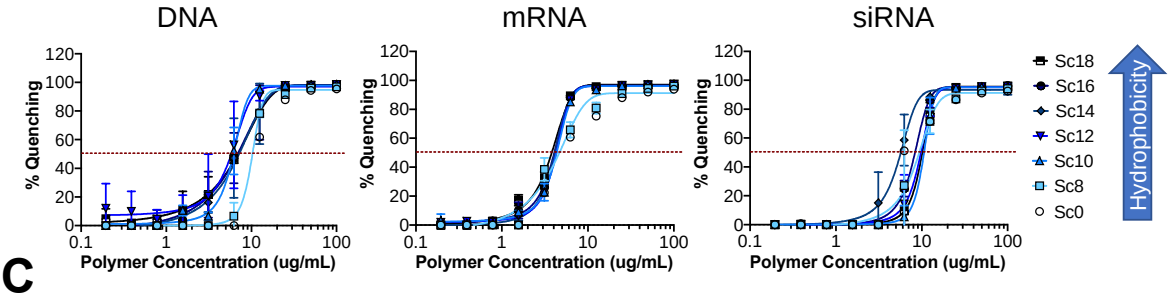

C

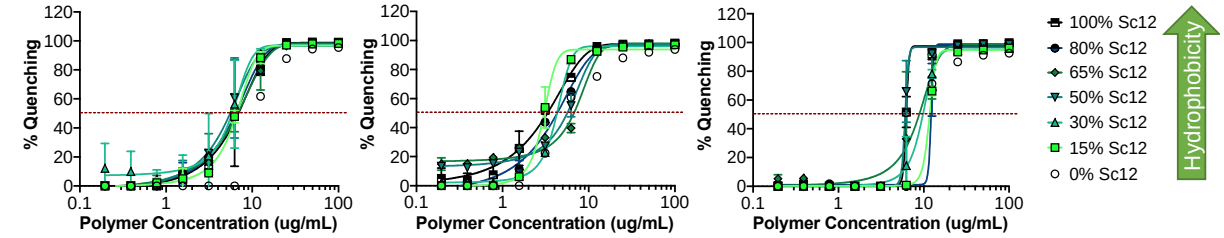

Figure S6. RiboGreen nucleic acid binding data. (A) Tabulated polymer IC50 of binding for polymers in the backbone variation series assessed with plasmid DNA, mRNA, and siRNA. **(B)** RiboGreen fluorescence quenching competitive binding curves for polymers in the alkyl chain length variation series. **(C)** Binding curves for polymers in the alkyl fraction variation series. Red line indicates 50% fluorescence quenching. Data shown as mean ± SD, *n* = 2.

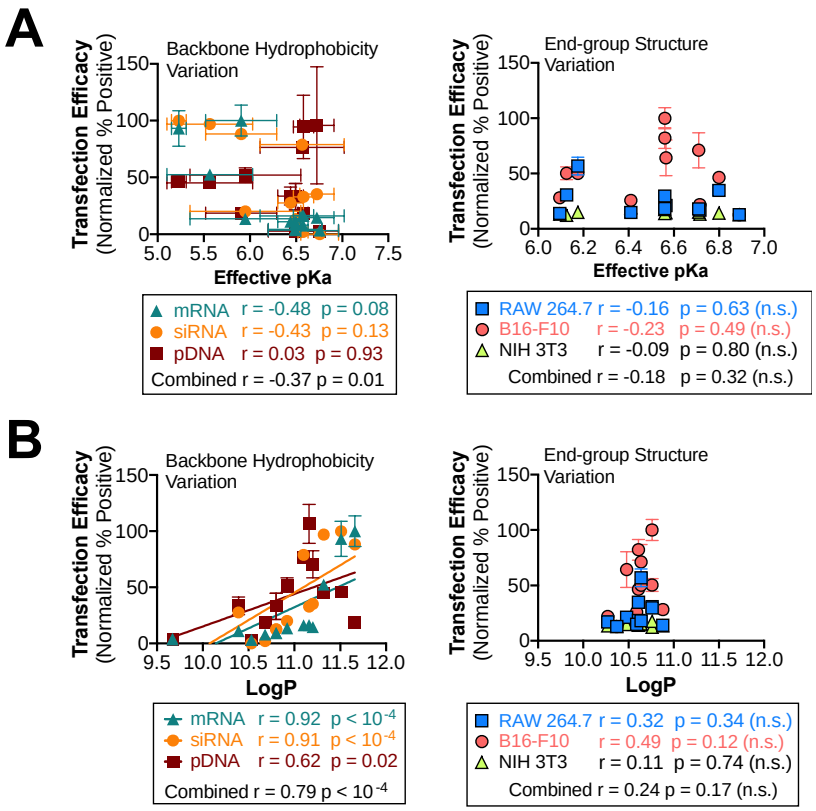

Figure S7. Correlations between *in vitro* transfection efficacy and polymer buffering capacity and hydrophobicity, respectively. Correlations between transfection efficacy and **(A)** polymer effective pKa in the physiological pH range or **(B)** predicted polymer LogP values of nanoparticles from backbone hydrophobicity variation polymers delivering different nucleic acid cargo (left) or end-group variation polymers delivering mRNA to different cell lines (right). Spearman's correlation was calculated to assess the strength of association between variable groups, and a line of best fit is shown for data sets with significant levels of correlation. Data shown as mean ± SD, $N = 4$.

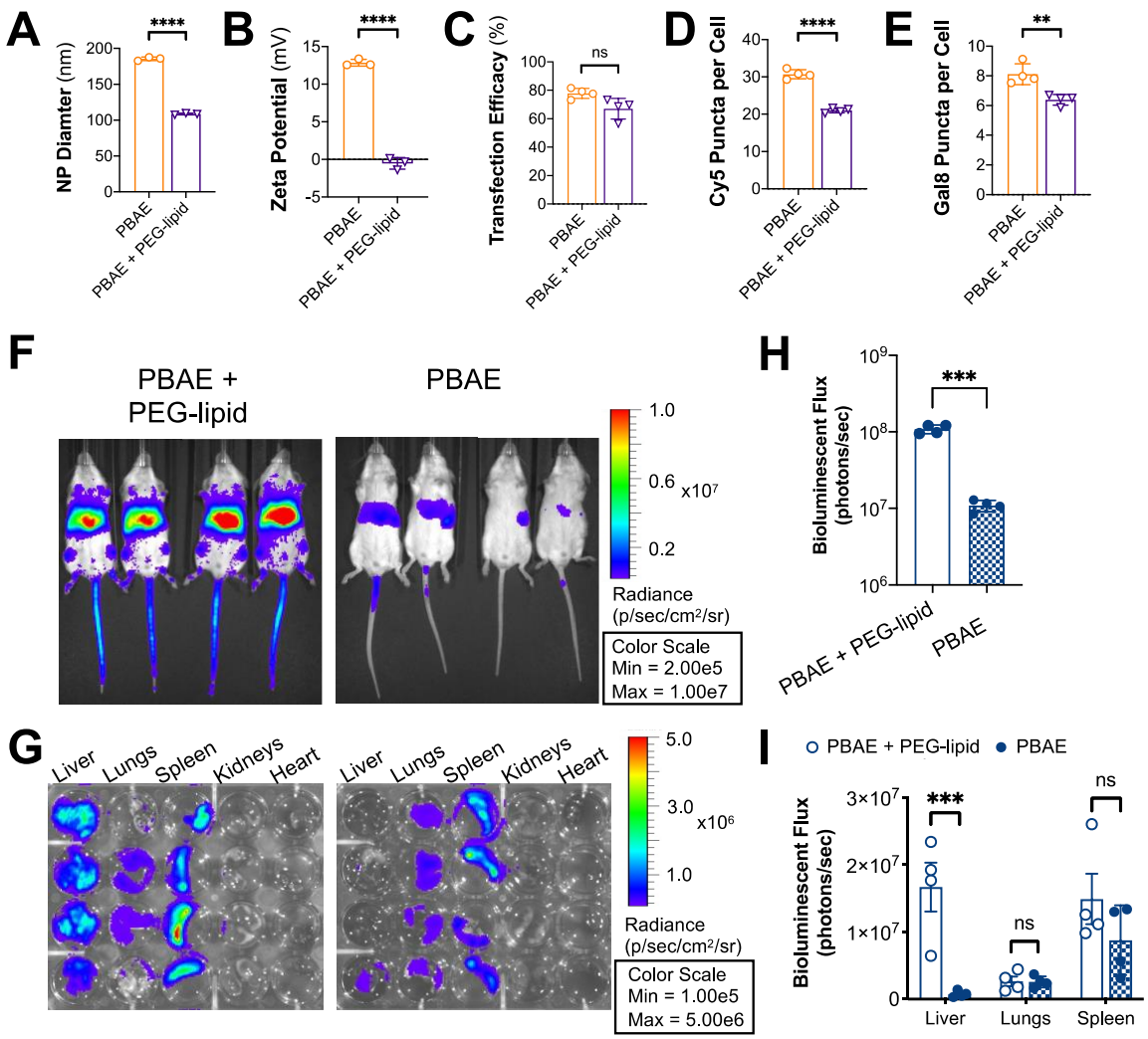

Figure S8. Effect of PEG-coating and dialysis on mRNA transfection. (A) Hydrodynamic diameter, **(B)** zeta potential, **(C)** mRNA transfection efficacy, **(D)** Cy5, and **(E)** Gal8 puncta count comparison between unshielded NPs (PBAE) and NPs dialyzed with DMG-PEG2k (PBAE + PEG-lipid). Cell assays were performed using B16-F10 cells and delivering 50 ng mRNA per 96-well. Data presented as mean ± SD, $N = 3$ for NP characterization studies and $N = 4$ for cell studies. IVIS bioluminescence imaging for **(F)** whole-body, live animals and **(G)** select organs in animals injected with dialyzed and PBAE or PBAE + PEG-lipid NPs. Readings taken 24 h after NP injection. Quantification of luminescence from **(H)** whole-body or **(I)** organ level images. Statistical significance calculated using Student's t-test with Welch's correction for **(A)-(E)** and **(H)** and 2-way ANOVA with Sidak's post-hoc analysis for (I). $^{**}P < 0.01$, $^{***}P < 0.001$, $^{****}P < 0.0001$. ns, not significant. ($N = 4$).

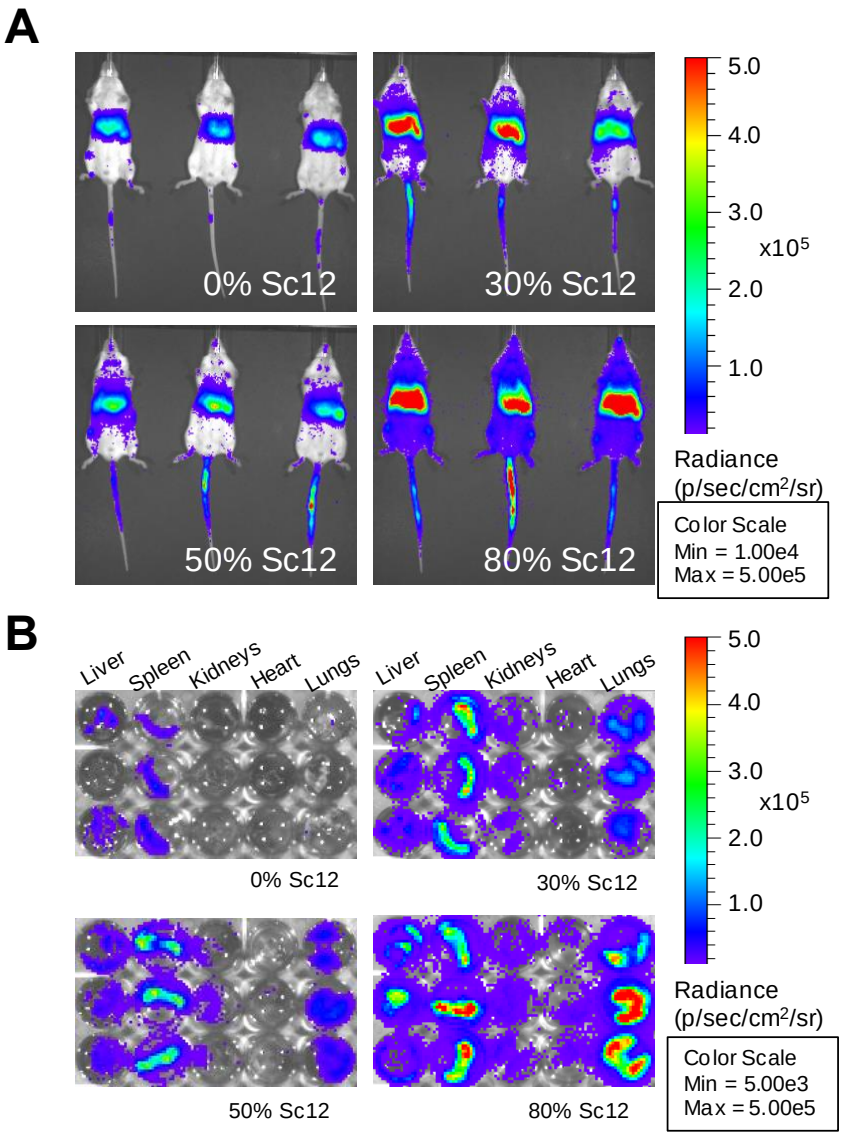

Figure S9. IVIS images of BALB/c mice treated with NPs formulated with fLuc mRNA and select polymers from the backbone hydrophobicity variation series. (A) Whole-body, live animal bioluminescence imaging. **(B)** Bioluminescence imaging of select organs. Readings taken 24 h after NP injection. (n = 3).

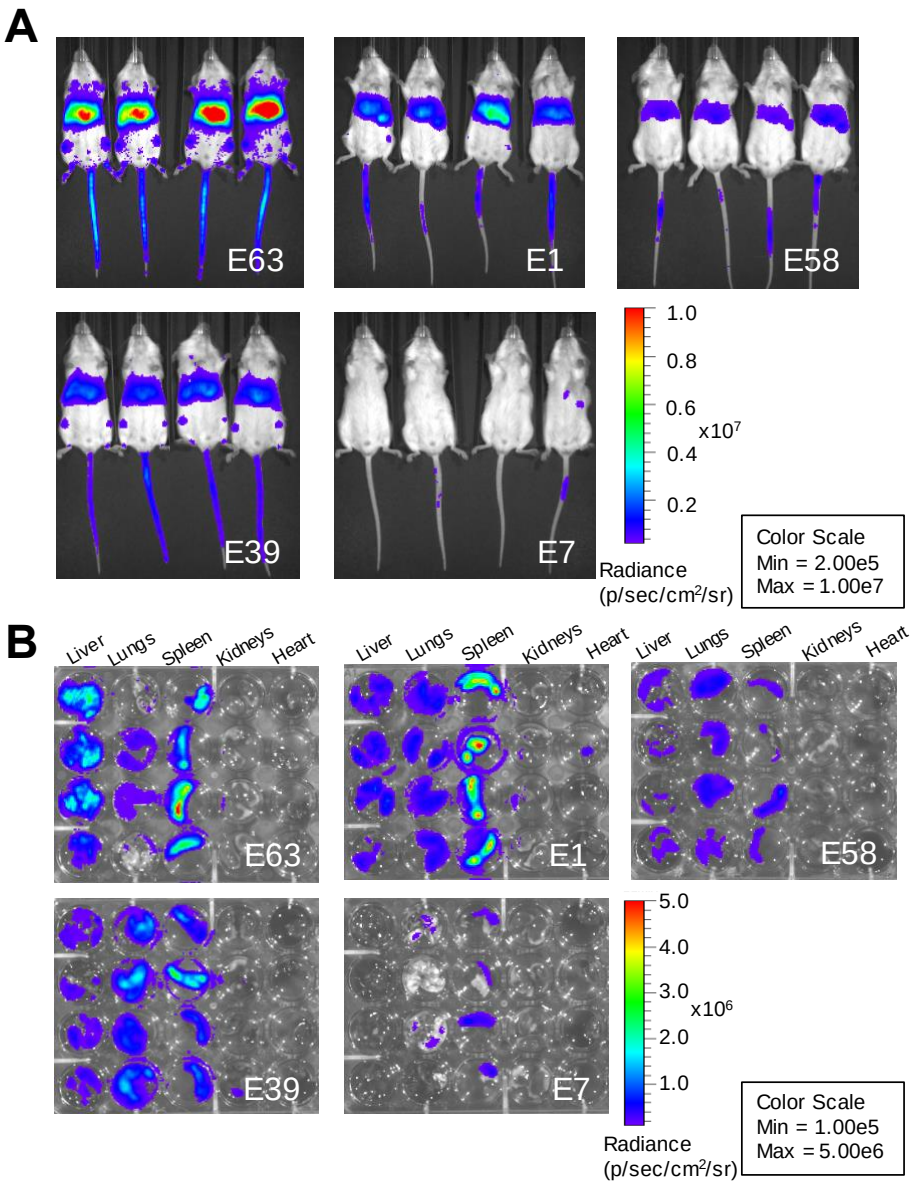

Figure S10. IVIS images of BALB/c mice treated with NPs formulated with fLuc mRNA and select polymers from the end-group variation series. (A) Whole-body, live animal bioluminescence imaging. **(B)** Bioluminescence imaging of select organs. Readings taken 24 h after NP injection. (n = 4).

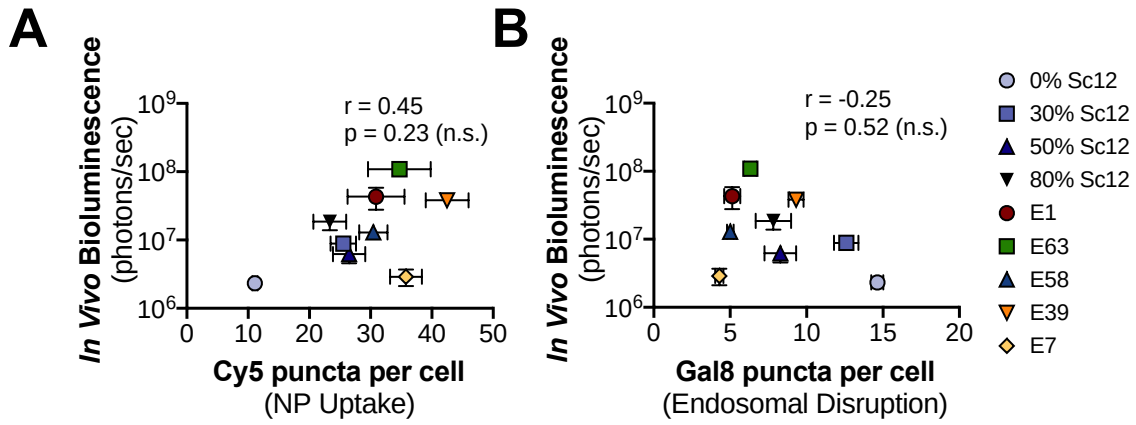

Figure S11. *In vivo* mRNA expression efficacy as a function of *in vitro* screening parameters. *In vivo* transfection efficacy as indicated by whole-body bioluminescence after IV injection of nanoparticles carrying fLuc mRNA was plotted against *in vitro* **(A)** nanoparticle uptake and **(B)** Gal8 endosomal disruption in B16 cells. Spearman's correlation was used to measure the strength of association between the two variables. Data presented as mean ± SD, $N \geq 3$.

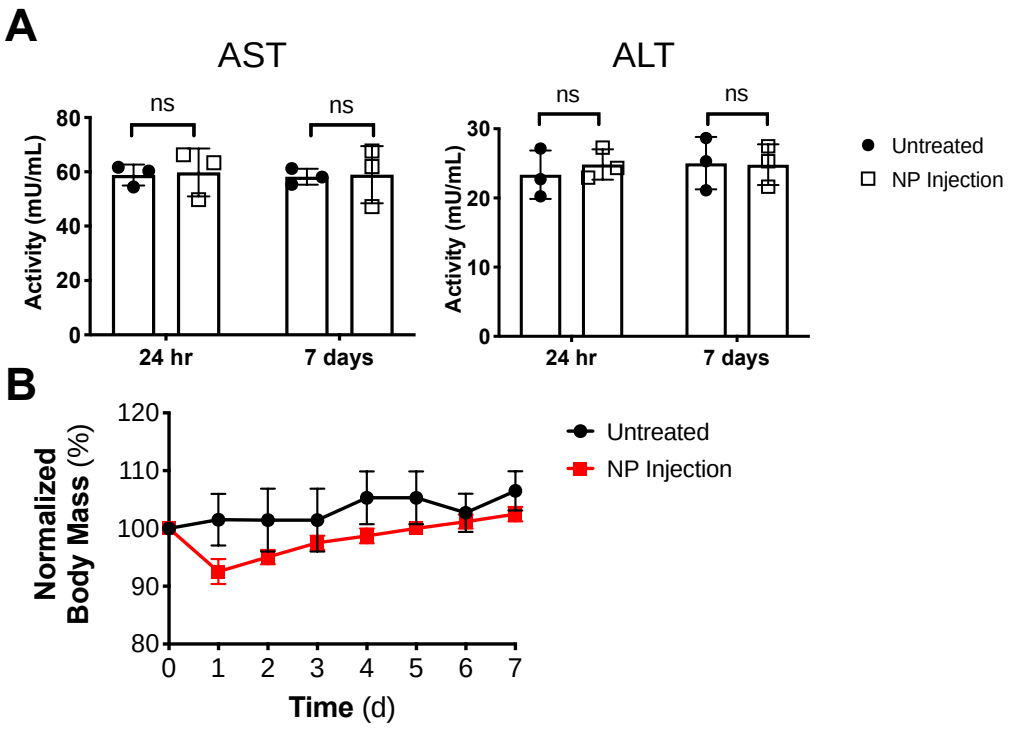

Figure S12. *In vivo* toxicity tests. *In vivo* toxicity as indicated by **(A)** liver enzyme tests and **(B)** normalized body mass after PEG-lipid coated 7-90,c12-63, 80%-Sc12 mRNA NP administration. Statistical significance assessed using 2-way ANOVA with multiple comparisons test between untreated animals and animals treated with a single I.V. mRNA NP injection at each time point. Differences in normalized body mass were not significant at any of the timepoints tested. Data presented as mean ± SD, $N = 3$.

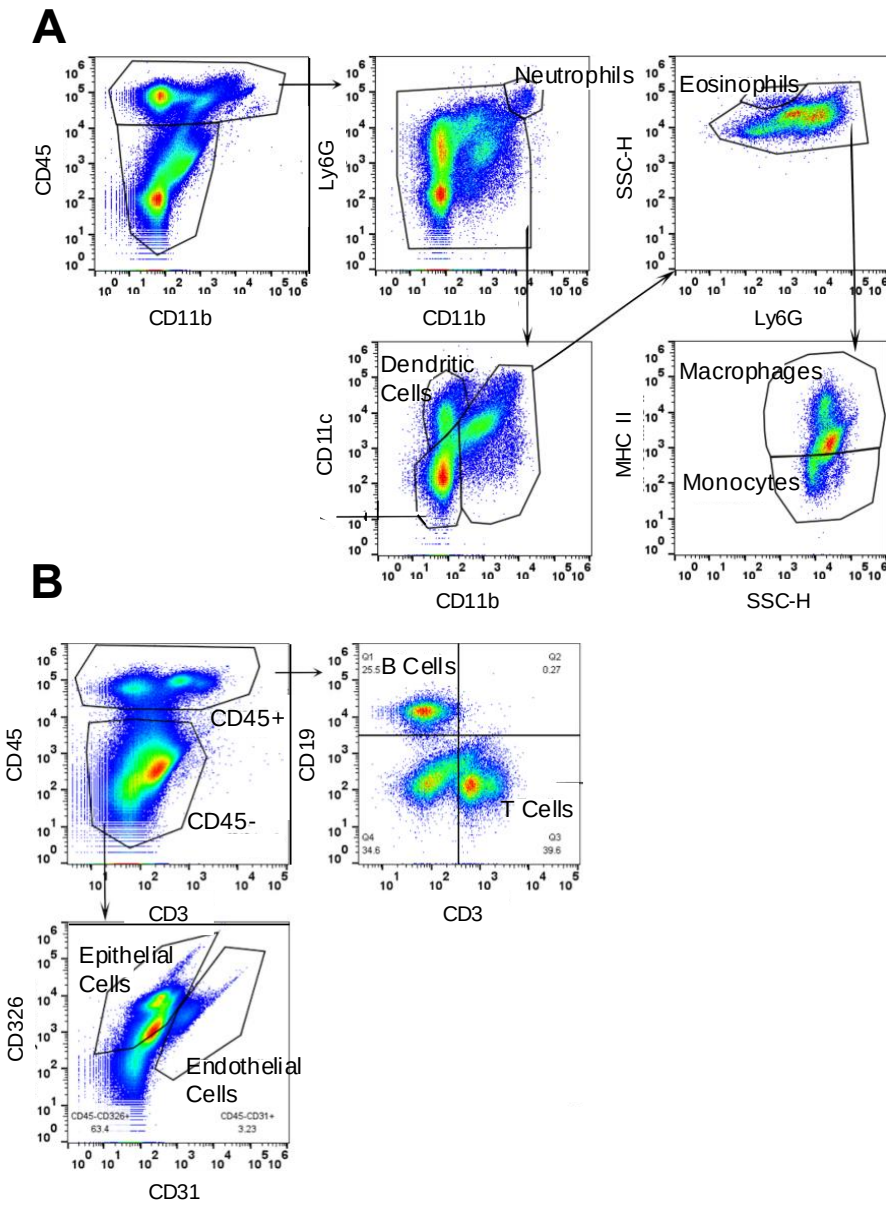

Figure S13. Flow cytometry gating strategies to identify cell type expression in Ai9 mice. Representative flow cytometry histograms to identify **(A)** various immune cell populations (panel 1) or **(B)** immune and non-immune cells (panel 2) in the liver.

Antigen	Color	Supplier	Clone	Dilution	Catalog No.	Lot No.
CD45	Brilliant Violet 421	Biolegend	30-F11	1:100	103134	B287242
CD11b	Alexa Fluor 488	Biolegend	M1/70	1:100	101217	B254608
CD11c	Allophycocyanin (APC)	Biolegend	N418	1:100	117310	B278343
I-A/I-E	Alexa Fluor 700	Biolegend	M5/114.14.2	1:100	107622	B264454
Ly6G	APC/Cyanine7 (Cy7)	Biolegend	1A8	1:100	127624	B264760
CD3	Alexa Fluor 488	Biolegend	17A2	1:80	100210	B284975
CD19	APC	Biolegend	6D5	1:100	115512	B284257
CD31/PECAM	Alexa Fluor 700	Biolegend	390	1:100	102443	B303280
CD326/EpCAM	APC/Cy7	Biolegend	G8.8	1:80	118218	B266989

Table S1. Antibody information for Ai9 flow cytometry experiments.